NFResNet: Multi-scale and U-shaped Networks for Deblurring

Tanish Mittal, Preyansh Agrawal, Esha Pahwa, Aarya Makwana

***Abstract*—Multi-Scale and U-shaped Networks are widely used in various image restoration problems, including deblurring. Keeping in mind the wide range of applications, we present a comparison of these architectures and their effects on image deblurring. We also introduce a new block called as NFResblock. It consists of a Fast Fourier Transformation layer and a series of modified Non-Linear Activation Free Blocks. Based on these architectures and additions, we introduce NFResnet and NFResnet+, which are modified multi-scale and U-Net architectures, respectively. We also use three different loss functions to train these architectures: Charbonnier Loss, Edge Loss, and Frequency Reconstruction Loss. Extensive experiments on the Deep Video Deblurring dataset, along with ablation studies for each component, have been presented in this paper. The proposed architectures achieve a considerable increase in Peak Signal to Noise (PSNR) ratio and Structural Similarity Index (SSIM) value.**

***Index Terms*—Multi-Scale, Unet, Deblurring, Fast Fourier Transform, ResBlock, Non-linear Activation Free Block, NFResnet, Charbonnier, Edge, Frequency Reconstruction**

I. Introduction

Image Deblurring has many applications. It can be used for better viewing space vehicles, satellites, and stars; medical imaging such as MRI; Iris recognition for facial verification; radar imaging; removing motion blur due to camera shake, etc. In this paper, we introduce a new NFResblock, which consists of the **N**AFBlock [1] and the **F**FT **Res**Block [2]. Using these additions, we introduce NFResnet based on MIMO-Unet and NFResnet+ based on the MultiScale Architecture. Our motivation behind these additions is based on high and low-frequency discrepancies between blurry and sharp image pairs.

Image deblurring has been a critical area of research, owing to an increase in the number of image and video datasets. However, the task comes with some challenges. Sharp images usually have an imbalance between low and high-frequency information, with the latter being in high quantity. CNNs, a significant part of ResBlocks, usually have a limited receptive field, especially in the early layers. Hence, a ResBlock might be advantageous in learning high-frequency components, but the low-frequency information will not be appropriately modelled. This challenge is tackled using the FFT Block [2] along with the edge and frequency reconstruction losses.

The NAF Block [1] is used to make the model more computationally efficient by dropping components that do not provide that much of a performance advantage with the amount of computational power they utilize, along with simplifying different components such as the activation function, normalization, and attention. Layer normalization is used to make training much smoother with different variations of learning rates along with preventing gradient explosion caused by the other components.

The main challenges in image deblurring include obtaining real-world motion-blurred datasets, long-range spatial dependency in the blur, wrong estimation of the blur, and suboptimal results when the blur is slight. Blurred images in the real world are usually too complex to be trained upon because of their non-uniformity. Synthetic image generation methods have been utilised to tackle this problem, including the dataset we will be using. We conduct our experiments on the frames of Deep Video Deblurring dataset (DVD) instead of GoPro dataset [3] owing to its diversity in the magnitude of blur and the real world scenarios depicted in the videos captured.

A. Contributions

Our major contributions are listed below:

- We aim to improve the existing method used for deblurring images. We have proposed a new ResBlock, NFResblock, which can be used in place of the simple ResBlock for better results.
- Using the proposed ResBlock, we have shown a significant improvement of 3.65% in PSNR, thereby establishing new state-of-the-art metric values for the chosen dataset (Results shown in Fig. 1)
- Extensive ablation experiments have been conducted to prove the significance of each of the individual components in the proposed networks.

B. Paper Organization

The paper has been organized in the following subsections: Section II discusses the previous essential work done in the field of image deblurring. Section III gives a detailed description of the architecture proposed, the components included in the network, and the loss functions used to supervise our results. In section IV, dataset details, experimental settings, and results have been provided, along with an analysis of those results. Finally, in section V, we conclude our study and discuss future directions.

II. Related work

This section highlights the previous key works done to solve the image deblurring problem. Our work focuses on blind

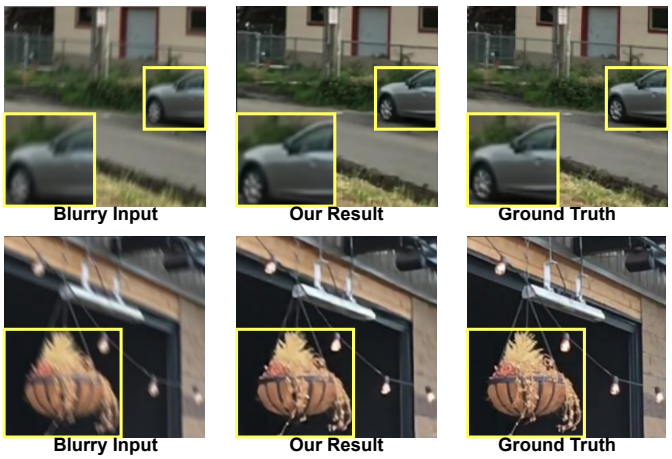

Fig. 1. Inference results of the NFResNet+ architecture proposed in this study. The blurry input, model's prediction, and ground truth sharp image are shown respectively for the two examples.

deblurring as most natural images come with no information about their blur kernel K. Without the knowledge of the blur kernel, we cannot use non-blind deblurring methods that involve deconvolutional and denoising networks. Blind deblurring methods mainly fall into two categories: kernel estimation and image-to-image regression.

To estimate spatially variant motion vectors, a neural network can be used to perform patch-wise classification and assign probabilities to several candidate motion vectors. A motion vector represents the translation and rotation of image patches, and we can associate several motion vectors with image patches to represent more complicated motions. The KCNN system [4] simplifies this by considering only linear translations. KCNN estimates the magnitude and direction of the motion vector for a given blurred patch and then assigns a probability to each translation and rotation, and the most likely is selected. The MBMF network [5] maps a blurred image to a motion field. MBMF has to be trained on a dataset consisting of blurred images and the corresponding motion vector fields consisting of translations along the x, y, and z axes, and a rotation around the z-axis, which are sufficient to simulate specific camera effects.

There are kernel-estimation blind deblurring methods that also consider working in the frequency domain. One such method was proposed in [6] that uses a combination of learning-based feature extraction and kernel estimation specific to image deconvolution. The major drawbacks of the kernel estimation methods are as follows:

- It is difficult to estimate complex motion kernels with a simple CNN network.
- A kernel estimation system that will deal with different types of blur is hard to design.

Direct Image-to-Image Regression (I2IR) methods have a benefit over Kernel-Estimation methods as they directly restore a latent sharp image without kernel estimation and thus avoid errors induced by an inadequate blur kernel. One example of I2IR - Multi-Scale CNN (MSCNN) [7] follows a coarse-to-fine approach. Coarse features are initially extracted by learning with images of reduced resolution. When features are found, they are passed through an up-convolution layer to increase the resolution to the following scale stage to extract more sophisticated features. In a network similar to MSCNN - SRN [8], the CNNs responsible for different scales share learnable parameters. Using fewer parameters to learn the same training dataset should allow a network to converge more quickly.

Generative models have also been deployed for the task of image deblurring. A single-scale training method based on a GAN - DeblurGAN [9], which has an encoder-decoder type CNN and a generator with residual layers, uses perceptual loss [10] as its content loss and a modified Wasserstein distance loss [11] for the adversarial loss. [12] introduced multi-scale discriminators to supply global and local structural details to the generator.

III. Proposed Methodology

In this section, we give a detailed description of the individual components used in the network and the overall architecture.

A. NFResblock

The proposed NFResBlock consists of two main components, namely FFT-ResBlock and NAF-Block. The following sub-sections describe them in detail.

1) FFT-ResBlock: We propose a new addition to the existing ResBlock, which helps us capture the information from the frequency domain. It is known that CNNs have a limited effective receptive field. As suggested by [13], it can be said that ResBlock instantiated by CNNs, may lack good abilities in modeling low-frequency information. Also, as mentioned by [14], blurry images tend to have more low-frequency information than sharp images. Thus, ResBlock's failure to capture low-frequency information is a significant constraint in reducing the inconsistency between the blurry and sharp images.

To tackle this problem, we add another branch based on a channel-wise Fast Fourier Transform (FFT). This helps us in capturing the global information in the frequency domain. First, the image is converted from spatial domain to frequency domain using FFT. Then, like a residual branch, frequency domain features are passed to convolution blocks followed by a non-linear activation function.

2) NAF-addition: NAF Block [1] is a novel convolutional building block of Nonlinear Activation Free Network, namely NAFNet [1]. To avoid over-complexity in the architecture, this block avoids using any activation functions like ReLU, GELU, Softmax, etc. hence keeping a check on the intra-block complexity of the network. We have conducted experiments with both the variations of the NAF-block introduced in [1].

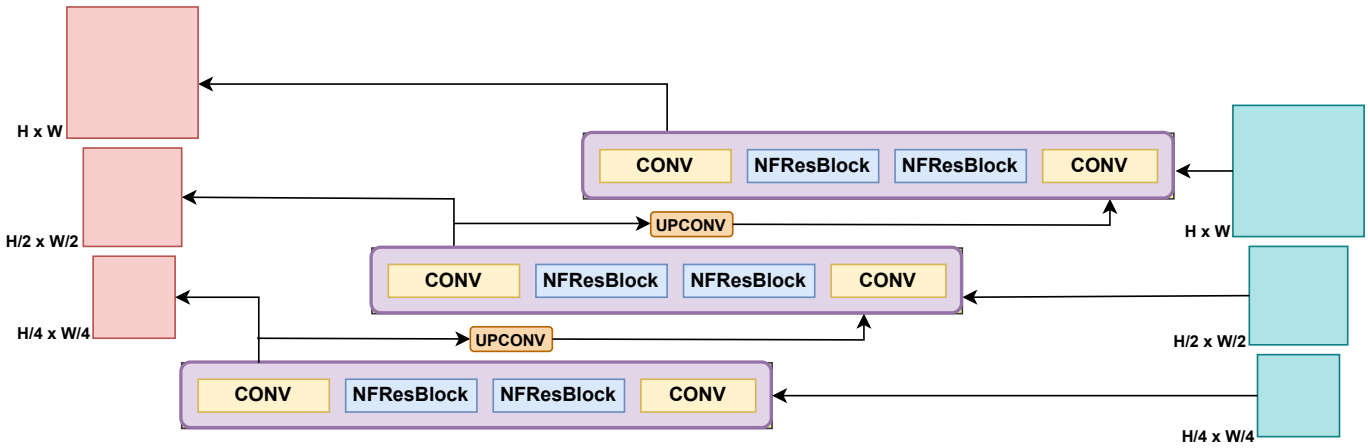

Fig. 2. NFResnet+ Architecture. It takes in the images of 3 different scales and produces sharp images at each level. Feature maps obtained at the end of each intermediate level are passed on to the upper level with the help of the upconv block.

Along with that, we have also conducted experiments using just the upper half and the lower half of the NAF-Block as illustrated in Fig. 3 (a) NAF-U and (c) NAF-D.

B. NFResNet

NFResNet is based on MIMO-Unet [15]. It utilizes a coarse-to-fine approach for single image deblurring compared to multi-scale architectures, which stack subnetworks and gradually increase the sharpness of images from bottom to top. It makes use of an encoder to make the training easier. It then uses a decoder similar to a multi-cascaded Unet architecture. Finally, it uses asymmetric fusion to merge these multi-scale features. The architecture consists of a single U-shaped block with 3 encoder and decoder blocks. The encoder is a multi-input block compared to other architectures, which only take a single input at the start. Similarly, the decoder is a multi-output block compared to other architectures that output a single image at the end.

The Multi-Input Single Encoder consists of a Convolution Block, a Feature attention module, and a Residual Block. The ResBlock is replaced by the NFResBlock containing the entire NAF structure along with the FFT operation (Fig. 3 (b)). It allows the model to learn critical information about the frequency domain and reduces the model's computational complexity. Features from the Encoder Block are combined with the blurry image's features. This helps in handling diverse image blurs [15]. Features are first extracted using a shallow convolution module which is then passed to the Feature attention module to emphasize or suppress the features and learn their spatial or channel importance. These are now sent to the NFResBlock for further refinement.

Asymmetric Feature Fusion, inspired by [16] allows information flow between different architecture scales. Each block takes the input of all the encoder blocks and combines the multi-scale features using a convolution layer. The output is then passed to the corresponding decoder block. This helps the decoder block in exploiting multi-scale features.

C. NFResnet+

NFResnet+ is similar to [17]. The choice of architecture is devised to solve the problem of dynamic scene deblurring. Conventional deblurring methods fail to solve the problem where the blur kernel is difficult to estimate. This leads to the failure of removing blur in the image. Our method involves a multi-scale architecture that restores sharp images when the blur is multi-sourced. The method also does not suffer from kernel-related problems arising in deblurring. The input and output are in the form of a batch of 3 images; each image is a downsampled version of the previous one. At each level, we have NFResBlocks, containing the NAF-U or the NAF-D structure of the NAF Block, sandwiched between convolution layers to form a ResNet structure. The central architecture involves using multiple ResNets at different scales where the output of the lower scale network is upconvolved to the input of the upper scale network. We have only included half of the NAF block - either the upper half or the lower half - as we observed that it was sufficient to get better results as compared to NFResNet with lower number of parameters. We also chose to go with multi-scale architecture (refer to Fig. 2) instead of a U-net architecture as it was a simplified solution of the same task.

D. Loss Functions

We train the model using three different loss functions and take a weighted sum with appropriate weights to get our final loss. We use $\mathbf{P}$ to denote the ground truth image and $\hat{\mathbf{P}}$ to denote the deblurred image resulting from our architecture. ε is a hyperparameter in the Charbonnier and Edge Loss, which is empirically set to a constant value 10^{-3}. The three losses are as follows:

1) Charbonnier Loss :

$$\mathfrak{L}_{char} = \sqrt{||\hat{\mathbf{P}} - \mathbf{P}||^2 + \varepsilon^2} \tag{1}$$

where $||\hat{\mathbf{P}} - \mathbf{P}||$ denotes the l_2 norm.

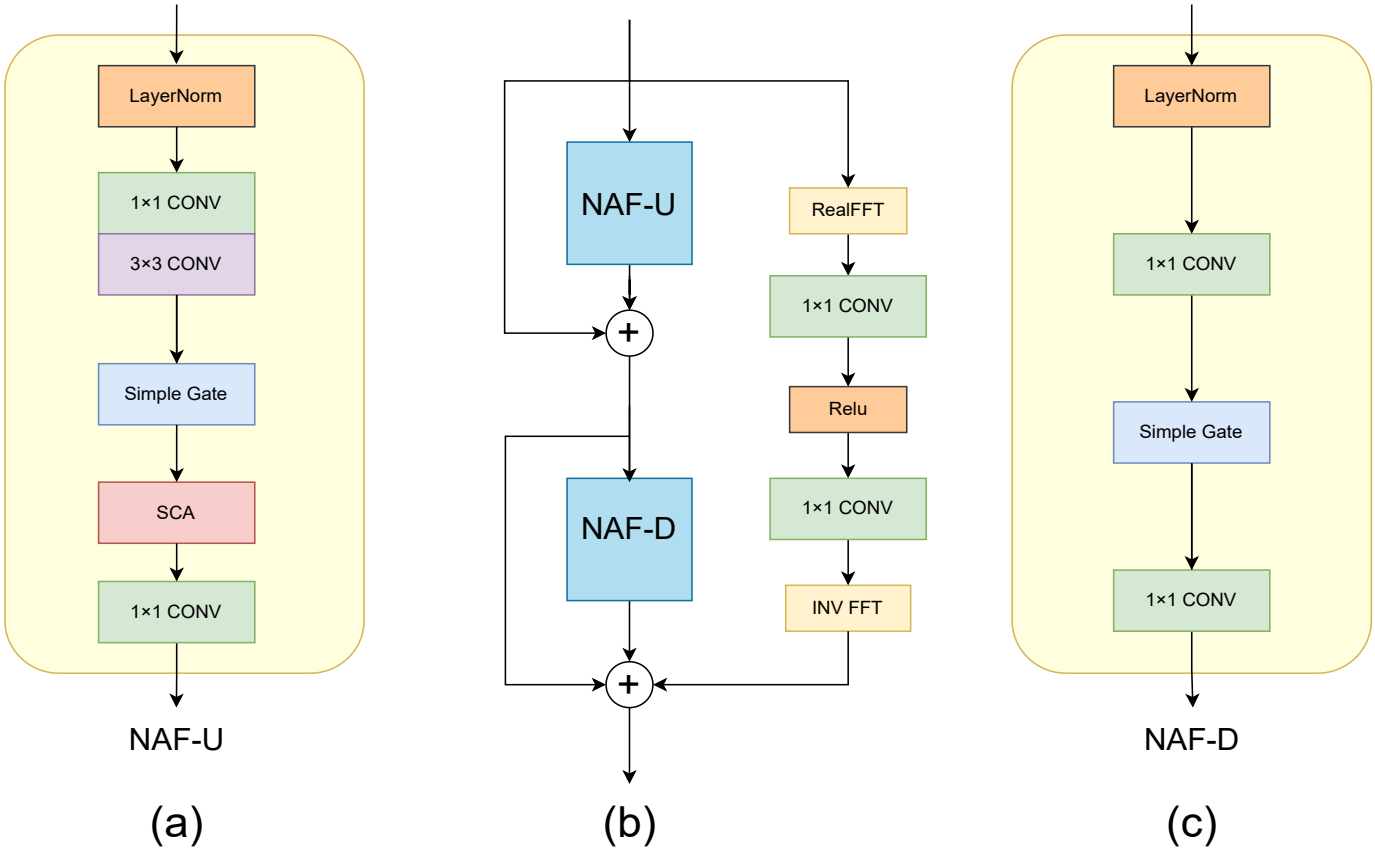

Fig. 3. (a) NAF-U (NAF-Upper) (b) It represents the complete structure of NFResblock. it contains one NAF branch, one skip connection, and one frequency branch. (c) NAF-D (NAF-Down)

The Charbonnier Loss provides edge-preserving regularization and makes the optimization easier due to its half-quadratic nature.

2) Edge Loss:

$$\mathfrak{L}_{edge} = \sqrt{||\Delta(\hat{\mathbf{P}}) - \Delta(\mathbf{P})||^2 + \varepsilon^2}, \tag{2}$$

where Δ denotes the Laplacian operator.
The Edge Loss is used to tackle the problem of loss of high-frequency details (such as edges) during downsampling. The standard upsampling algorithms do not preserve this information.

3) Frequency Reconstruction Loss:

$$\mathfrak{L}_{fft} = ||\mathbb{FT}(\hat{\mathbf{P}}) - \mathbb{FT}(\mathbf{P})||_1, \tag{3}$$

where $\mathbb{FT}$ represents the FFT operation.
The Frequency Reconstruction loss is used to preserve information regarding low and high-frequency details in the frequency domain.

Our final loss then becomes: $\mathfrak{L} = \mathfrak{L}_{char} + \alpha_1 \mathfrak{L}_{edge} + \alpha_2 \mathfrak{L}_{fft}$, where α_1 is set to 0.05 and α_2 is set to 0.01 empirically. These are hyperparameters used to control the dominance of a particular loss.

IV. Experimental Results

To discuss the setting and the outcome of our proposed model's approach, this section contains a description of the dataset chosen in Section IV-A, the experimental settings in Section IV-B, the metrics used for evaluation in Section IV-C and a discussion on the results obtained in Section IV-D and IV-E.

A. Dataset details

We conduct our experiments on the DVD dataset [18]. Sharp videos in the dataset were captured at a frame rate of 240 fps, and every eighth frame was subsampled to store the 30 fps ground truth sharp frame. The initial seven frames are averaged to generate a realistic motion blur. To avoid ghosting artifacts created by averaging, optical flow was computed between adjacent high fps frames, and an additional ten evenly spaced inter-frame images were generated, which were then averaged together. Videos were shot using iPhone 6s, GoPro Hero 4 Black, and Canon 7D. Multiple devices were used to avoid bias towards a specific capturing device that may generate videos with some unique features. The dataset contains 6708 synthetic blurry frames and corresponding sharp frames. Train: Test ratio in our experiments was kept as 80:20.

Method	PSNR	SSIM	Year
DVD [18]	25.44	0.8412	2017
MobileNetv2 [19]	28.54	0.8654	2019
Qi *et al.* [20]	28.72	0.8702	2020
Tao *et al.* [8]	29.55	0.8822	2018
Zhang *et al.* [21]	29.01	0.8732	2019
Ye *et al.* [22]	30.81	0.9045	2020
Xia *et al.* [23]	30.92	0.9057	2022
NFResNet (**Ours**)	31.95	0.9052	2022
NFResNet+ (**Ours**)	32.05	0.8938	2022

TABLE I
QUANTITATIVE DEBLURRING PERFORMANCE COMPARISON ON THE DVD DATASET WITH THE PREVIOUS WORKS. BLUE NUMERICAL VALUES REPRESENT THE SECOND HIGHEST VALUE, WHEREAS RED REPRESENTS THE HIGHEST VALUE OF THE METRIC.

S.no.	Multi-scale Net	NAF-type	NAF-L	NAF-U	FFTResBlock	Loss	PSNR	SSIM
1	✓	✗	✗	✗	✗	L1	30.130	0.849
2	✓	Baseline	✓	✓	✗	L1	30.670	0.864
3	✓	Baseline	✓	✓	✗	L1, EDGE, FFT	30.887	0.862
4	✓	Improved	✓	✓	✗	L1, EDGE, FFT	31.579	0.883
5	✓	Baseline	✓	✗	✓	L1, EDGE, FFT	32.046	0.891
6	✓	Improved	✓	✗	✓	L1, EDGE, FFT	32.050	0.894

TABLE II
QUANTITATIVE DEBLURRING PERFORMANCE OF NFRESNET+ FOR DIFFERENT VARIATIONS. "BASELINE" NAF-TYPE REFERS TO THE BASELINE NAF-BLOCK INTRODUCED IN [1] AND "IMPROVED" REFERS TO THE IMPROVED VERSION OF THE BASELINE USING A SIMPLE GATE, AS INTRODUCED IN [1].

B. Experimental Settings

To make the model generalized to different types of scenarios and to prevent overfitting, the images were randomly flipped, horizontally and vertically, and rotated by 90 degrees. For augmentation in colour, RGB channels were randomly permuted. To account for cases of image degradation, a number was chosen randomly in the range [0.5, 1,5] and then multiplied by the saturation level in the HSV colourspace. Gaussian noise was added, wherein the standard deviation of the noise is also randomly sampled using a Gaussian distribution $N(0, (2/255)^2)$. Values outside [0, 1] were clipped. To keep the range of input and output between [-0.5, 0.5] so that they are zero-centered, 0.5 was subtracted from their values.

Training of the dataset was carried out till 40 epochs in each setting, after which we observed the convergence of loss values. The model was compiled using the Pytorch backend. Adam optimizer with a learning rate of 10^{-4}, β_1 and β_2 with a value of 0.9 and 0.999 was used. 40 blocks and 19 blocks were used at each level in NFResNet and NFResNet+ respectively.

C. Evaluation Metrics

Peak Signal to Noise Ratio (PSNR) and Structural Similarity Index (SSIM) are the standard metrics we report for all our experiments.

S.no.	MIMO-Unet	FFTBlock	Loss	PSNR	SSIM
1	✓	✓	L1	30.5970	0.8783
2	✓	✓	L1, FFT	31.0251	0.8991
3	✓	✓	L1, Edge	31.7590	0.9010
4	✓	✓	L1, FFT, Edge	31.9503	0.9052

TABLE III
QUANTITATIVE DEBLURRING PERFORMANCE OF NFRESNET FOR DIFFERENT COMBINATIONS OF LOSS FUNCTIONS.

S.no.	Loss-type	Conv-type	PSNR	SSIM
1	Single	normal	32.050	0.894
2	Single	dilated	32.053	0.895
3	Multi	normal	32.096	0.893
4	Multi	dilated	32.097	0.898

TABLE IV
QUANTITATIVE DEBLURRING PERFORMANCE OF NFRESNET+ FOR DIFFERENT CONVOLUTION TYPES AND LOSS IMPLEMENTATION SCALES. A "NORMAL" CONVOLUTION REFERS TO A DILATION RATE OF 1, WHEREAS A "DILATED" CONVOLUTION REFERS TO A DILATION RATE OF 2.

D. Discussion and Comparison

As seen in TABLE I, our proposed architectures achieve the best and the second best performance for PSNR and SSIM, respectively, as compared to the previous works. We observe a significant increase of 25.98% when compared with the original dataset baseline [18]. Both [18] and [19] do not exploit the attention mechanisms in their models, which helps us focus on the specific blurry areas in the image. Moreover, [19] has an unstable training procedure, which is one of the technical disadvantages of using generative adversarial networks. [20] uses an attention mechanism to tackle non-uniform blur through a feature fusion block. However, we remove the heavy pixel attention and channel attention model and use a simple gate in NAF-D and simple channel attention in NAF-U to capture the long-range dependencies to achieve an 11.59% increase in PSNR value. Our NFResNet alone surpasses the metrics obtained by [8], [21] and [22] owing to the feature attention and ResBlock modules and the interconnected architecture that shares the information across different feature maps obtained at different scales.

To make our model even more straightforward, we remove feature attention modules, shallow convolutional modules, extra skip connections and the encoder-decoder architecture as proposed in MIMO-Unet [15]. For the remaining multi-input-multi-output network, we use a group of convolution blocks containing normal convolutions and NFResBlocks (refer Fig. 3) and term it as NFResNet+. As a result, NFResNet has 13.84M parameters, whereas NFResNet+ (containing NAF-Down block) has 13.60M parameters. We do not utilize the complete NAF structure in our NFResNet+ as we hypothesized that having one feature attention layer was enough for the model to focus on the blurry areas. We observed that a better value of PSNR was obtained in the case of NFResNet+ with fewer parameters. A slight decrease was also observed in the value of SSIM compared to NFResNet,

which could be because of the removal of additional feature attention modules and skip connections.
The visual results obtained for both NFResNet and NFResNet+ are given in Fig. 4 and 5.

E. Ablation Studies

To prove the importance of each component in our network, we repeat our experiments with different components in NFResNet+ and report the results of the metric values obtained in TABLE II. Using a simple multi-scale network (S.no. 1) and just L-1 loss gave the worst performance out of all the experiments conducted. Using the baseline and improved NAF-block introduced in [1], without incorporating the FFT skip connection (S.no. 2, 3 and 4), supervised with all three losses, gave better results. As expected, the improved version of the NAF-block gave better results and hence was used in all the other experiments with NFResNet and NFResNet+. Surprisingly, using just NAF-Down with the FFT module (S.no. 5 and 6) gave a better performance than using both NAF-Up and NAF-Down (S.no. 3 and 4). This could be due to the simple gate layer added in the NAF-Down architecture and the FFT operations used in the FFT skip connection, which takes care of the high frequency and low-frequency details, while the simple gate calculates the importance of features.

The model was also trained on different combinations of loss functions, as seen in TABLE III. The best result is obtained by using all three loss functions for supervision.

We also conducted experiments with multi-scale loss by replacing a normal convolution with a dilated convolution layer in the NFResNet+ network and reported the results in TABLE IV. The results obtained align with the concept of dilated convolutions as they increase the receptive field. Along with this, calculating loss at each scale improves the supervision while training the model, leading to a better testing result. Hence, we obtain the best result by adding dilation and multi-scale loss (S.no. 4).

V. Conclusion

In this study, we introduced NFResBlock and modified U-Net and Multi-scale architectures. Unlike other methods, which do not use the parameters efficiently to get a high PSNR and SSIM value, we achieve state-of-the-art results on a well-known deblurring dataset, DVD. In addition, our NFResNet and NFResNet+ can be applied to other image restoration tasks that involve preserving high-frequency and low-frequency details. Quantitative and qualitative results demonstrate that our model performs well against previous image deblurring methods. Our method could also be deployed on edge devices as it is efficient and accurate. Future work would include extending our study to other image deblurring datasets and further to the video deblurring task.

References

[1] L. Chen, X. Chu, X. Zhang, and J. Sun, "Simple baselines for image restoration," *arXiv preprint arXiv:2204.04676*, 2022.

[2] X. Mao, Y. Liu, W. Shen, Q. Li, and Y. Wang, "Deep residual fourier transformation for single image deblurring," *arXiv preprint arXiv:2111.11745*, 2021.

[3] S. Nah, T. H. Kim, and K. M. Lee, "Deep multi-scale convolutional neural network for dynamic scene deblurring," in *CVPR*, July 2017.

[4] J. Sun, W. Cao, Z. Xu, and J. Ponce, "Learning a convolutional neural network for non-uniform motion blur removal," in *Proceedings of the IEEE conference on computer vision and pattern recognition*, 2015, pp. 769–777.

[5] D. Gong, J. Yang, L. Liu, Y. Zhang, I. Reid, C. Shen, A. Van Den Hengel, and Q. Shi, "From motion blur to motion flow: A deep learning solution for removing heterogeneous motion blur," in *Proceedings of the IEEE conference on computer vision and pattern recognition*, 2017, pp. 2319–2328.

[6] C. J. Schuler, M. Hirsch, S. Harmeling, and B. Schölkopf, "Learning to deblur," *IEEE transactions on pattern analysis and machine intelligence*, vol. 38, no. 7, pp. 1439–1451, 2015.

[7] S. Nah, T. Hyun Kim, and K. Mu Lee, "Deep multi-scale convolutional neural network for dynamic scene deblurring," in *Proceedings of the IEEE conference on computer vision and pattern recognition*, 2017, pp. 3883–3891.

[8] X. Tao, H. Gao, X. Shen, J. Wang, and J. Jia, "Scale-recurrent network for deep image deblurring," in *Proceedings of the IEEE conference on computer vision and pattern recognition*, 2018, pp. 8174–8182.

[9] O. Kupyn, V. Budzan, M. Mykhailych, D. Mishkin, and J. Matas, "Deblurgan: Blind motion deblurring using conditional adversarial networks," in *Proceedings of the IEEE conference on computer vision and pattern recognition*, 2018, pp. 8183–8192.

[10] J. Johnson, A. Alahi, and L. Fei-Fei, "Perceptual losses for real-time style transfer and super-resolution," in *European conference on computer vision*. Springer, 2016, pp. 694–711.

[11] M. Arjovsky, S. Chintala, and L. Bottou, "Wasserstein generative adversarial networks," in *International conference on machine learning*. PMLR, 2017, pp. 214–223.

[12] J. Liu, W. Sun, and M. Li, "Recurrent conditional generative adversarial network for image deblurring," *IEEE Access*, vol. 7, pp. 6186–6193, 2018.

[13] H. Wang, X. Wu, Z. Huang, and E. P. Xing, "High frequency component helps explain the generalization of convolutional neural networks," 2019. [Online]. Available: https://arxiv.org/abs/1905.13545

[14] X. Mao, Y. Liu, W. Shen, Q. Li, and Y. Wang, "Deep residual fourier transformation for single image deblurring," 2021. [Online]. Available: https://arxiv.org/abs/2111.11745

[15] S.-J. Cho, S.-W. Ji, J.-P. Hong, S.-W. Jung, and S.-J. Ko, "Rethinking coarse-to-fine approach in single image deblurring," 2021. [Online]. Available: https://arxiv.org/abs/2108.05054

[16] S.-W. Kim, H.-K. Kook, J.-Y. Sun, M.-C. Kang, and S.-J. Ko, "Parallel feature pyramid network for object detection," in *Computer Vision – ECCV 2018*, V. Ferrari, M. Hebert, C. Sminchisescu, and Y. Weiss, Eds. Cham: Springer International Publishing, 2018, pp. 239–256.

[17] S. Nah, T. H. Kim, and K. M. Lee, "Deep multi-scale convolutional neural network for dynamic scene deblurring," *CoRR*, vol. abs/1612.02177, 2016. [Online]. Available: http://arxiv.org/abs/1612.02177

[18] S. Su, M. Delbracio, J. Wang, G. Sapiro, W. Heidrich, and O. Wang, "Deep video deblurring for hand-held cameras," in *Proceedings of the IEEE conference on computer vision and pattern recognition*, 2017, pp. 1279–1288.

[19] O. Kupyn, T. Martyniuk, J. Wu, and Z. Wang, "Deblurgan-v2: Deblurring (orders-of-magnitude) faster and better," in *Proceedings of the IEEE/CVF International Conference on Computer Vision*, 2019, pp. 8878–8887.

[20] Q. Qi, J. Guo, and W. Jin, "Attention network for non-uniform deblurring," *IEEE Access*, vol. 8, pp. 100 044–100 057, 2020.

[21] H. Zhang, Y. Dai, H. Li, and P. Koniusz, "Deep stacked hierarchical multi-patch network for image deblurring," in *Proceedings of the IEEE/CVF Conference on Computer Vision and Pattern Recognition*, 2019, pp. 5978–5986.

[22] M. Ye, D. Lyu, and G. Chen, "Scale-iterative upscaling network for image deblurring," *IEEE Access*, vol. 8, pp. 18 316–18 325, 2020.

[23] H. Xia, B. Wu, Y. Tan, X. Tang, and S. Song, "Mfc-net: Multi-scale fusion coding network for image deblurring," *Applied Intelligence*, pp. 1–18, 2022.

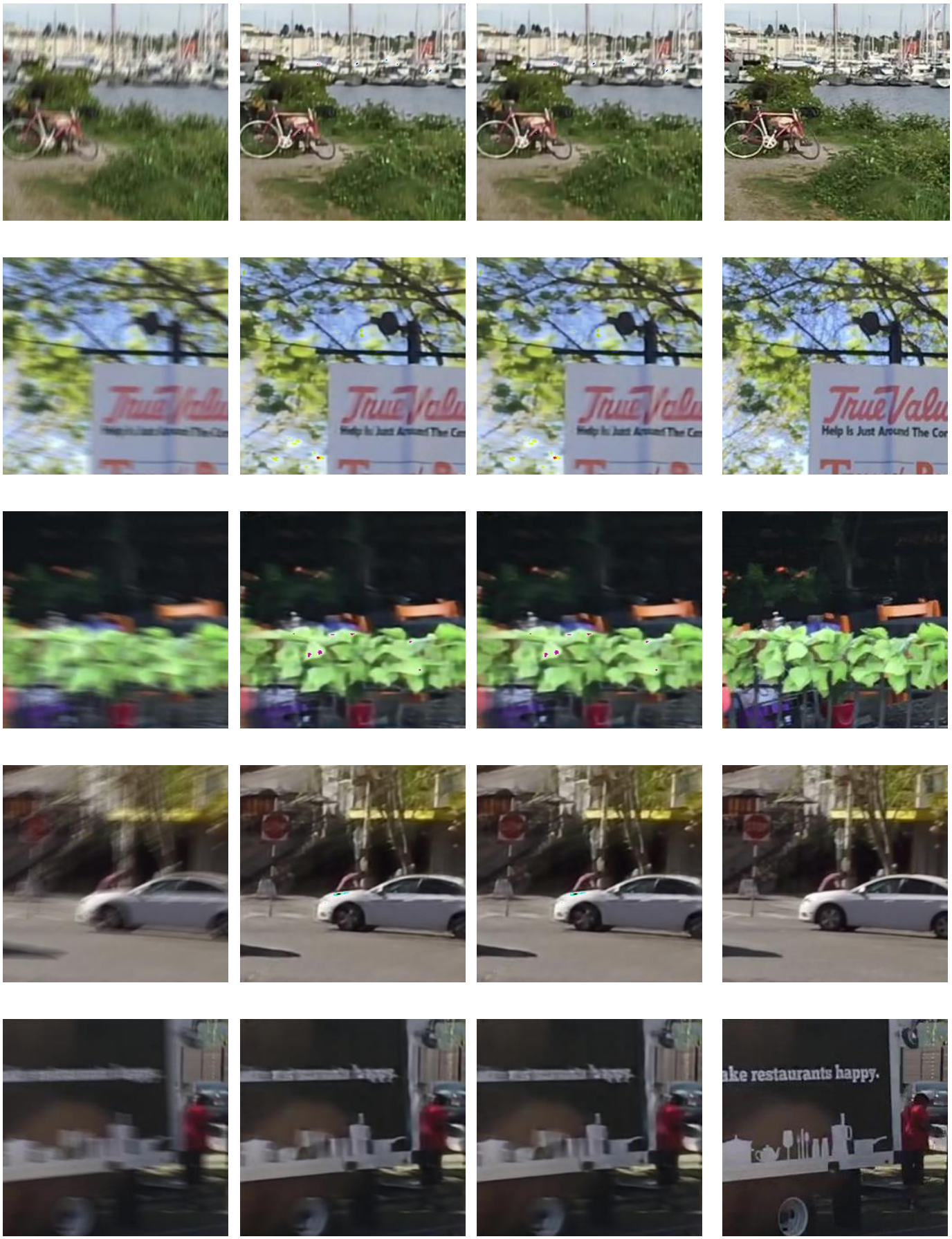

Fig. 4. Test Results on the DVD dataset.

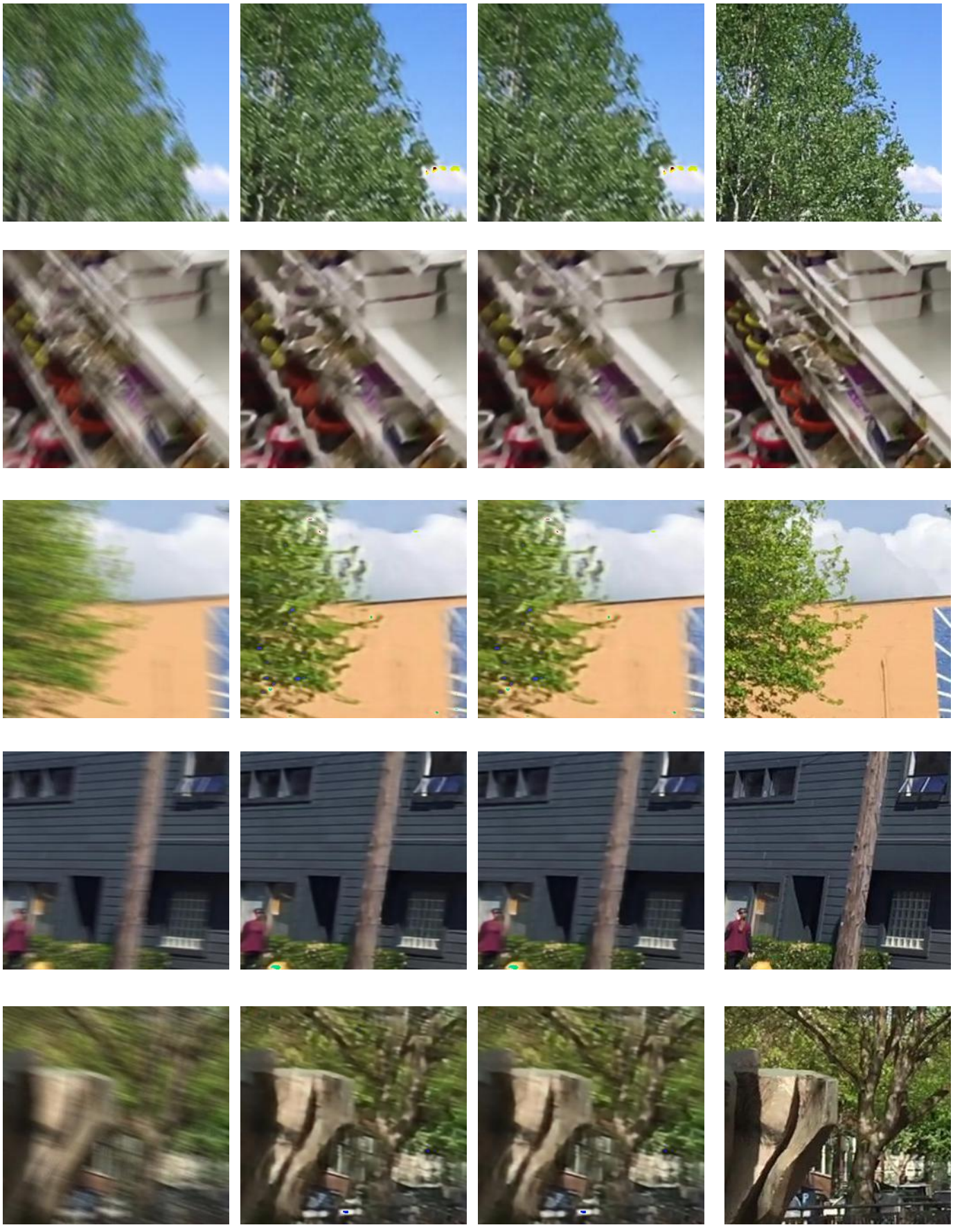

Fig. 5. Test Results on the DVD dataset.